Wake vortex alleviation by differential and oscillating flap setting: a comparative numerical and experimental study

G. Voß, C. v. Carmer, R. Konrath, E. Stumpf, C.-P. Krückeberg, H.Meyer, H. Mattner

Deutsches Zentrum für Luft- und Raumfahrt e.V.
in der Helmholtz-Gemeinschaft

Institut für Aerodynamik und Strömungstechnik

Lilienthalplatz 7, 38108 Braunschweig
Bunsenstraße 10, 37073 Göttingen

The work in this publication was done in the framework of Wirbelschleppe II project, which was funded by DLR.

1 Abstract

In this article the results of numerical calculations and experimental studies on wake vortex alleviation using Differential Flap Setting (DFS) and Oscillating Flap Setting (OFS) by means of a principle model with rectangular wing as a vortex generator should be presented. The numerical part of the examination was made as an Euler-computation provided with flow solver TAU, the experiment was performed in a water towing tank at DLR Göttingen. The comparison of different configurations according to flap setting, trigger frequency and influence of HTP vortex was conducted in this paper. Both numerical and experimental investigations have shown that it is possible to affect the wake vortex development using configurative methods on lift devices. Further investigations have to be done to calculate the circulation and the rolling moment influence on following aircraft.

2 Introduction

An aircraft generates a wake flow which is called wake vortex, trailing vortices or wake turbulence. This is hazardous for following aircraft while encountering the strong wake vortices. Since the strength of the wake vortices increases with increasing lift (or rather the weight) of the aircraft, this problem is serious for high capacity airliners during take off and landing. The research on wake vortices was of interest for several decades. Presently, the growth of air traffic has led to the construction of very large aircraft which produces very strong wake vortices. Increase of the separation distances might compensate the advantage of larger transport capacity. Hence, it is necessary to develop new concepts to make a forecast of vortex occurence in order to avoid encountering or adjust the effect on aircraft behaviour while encountering. Futhermore one approach to optimize the separation standards is the wake vortex alleviation by configurative methods on aircraft lift devices. This wake vortex control has become one challenging task in civil aviation concerning flight safety and increasing airport efficiency. The objective of the investigations conducted in this work is the excitation of vortex instabilities of the vortex system behind a lift body.

3 Theory

3.1 Vortex parameter

The wake of an aircraft is basically a vortex-dominated flow. Within the wake one can find vortex layer shed from the trailing edges and single vortices which are coming from the side edges of the lift devices. Within a distance of about ten spans behind the aircraft the complex wake topology is reduced to a system of few counter-rotating vortices.

Some important vortex parameters should be characterized as follows. In common a vortex is defined by a rotational motion of particles into a single focus. The trajectories of the particles needn`t be circular and in the case of spatial vortices not necessarily closed.

The vortex motion of the particles can be described by a distribution of the components of either the velocity vector v or the vorticity vector ω. Vorticity is here defined as the rotation of the velocity in a point in space:

(1) $$\vec{\omega} = \nabla \times \vec{v}$$

In the special case of a planar vortex field the vortex flow is two-dimensional. The vorticity vector in yz-plane is reduced to the axial component of ω:

(2) $$\omega_x = \frac{\partial v}{\partial z} - \frac{\partial w}{\partial y}$$

The integration of the axial vorticity ω_x is a measure for the magnitude of a vortex. It is called circulation. The circulation Γ_0 in yz-plane is defined as:

(3) $$\Gamma_0 = \int_{-\infty}^{\infty}\int_{-\infty}^{\infty} \omega_x dydz$$

FIG. 1 shows a sketch of a counter-rotating 4-vortex system. The main parameters to describe a 4-vortex system are the ratio of spacing b_1/b_0 and the ratio of circulation Γ_1/Γ_0 of both vortex pairs. The behaviour of a 4-vortex system depends on the value of the vortex parameter. With Donaldson-Bilanin diagram (FIG. 2) one can give a prediction how the motion of the vortices will appear.

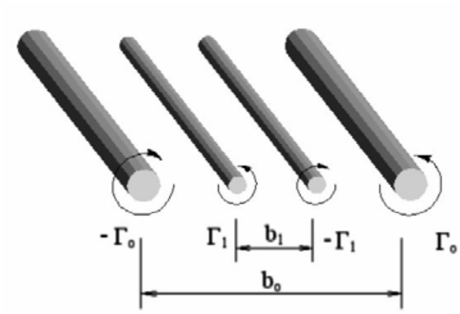

FIG. 1: Counter-rotating 4-vortex-system with spacing b and Circulation Γ

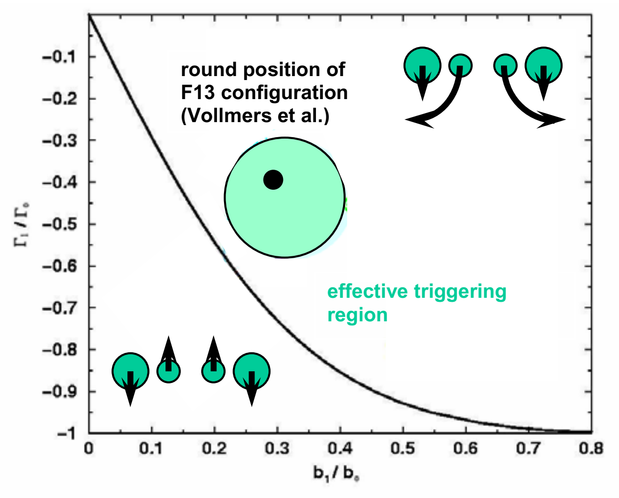

FIG. 2: Donaldson-Bilanin-diagram

3.2 Vortex instabilities

The natural vortex decay is based on vortex instabilities. One can differ between centrifugal and cooperative instabilities. In this work the main focus should be set on cooperative instabilities.
Vortex pairs may exhibit a kind of instability which is based on interactions between vortex systems over the symmetry plane. Due to that fact these instabilities are called cooperative instabilities. The requirement for that kind of instability of a vortex is a radial deformation field i.e. induced by a neighbor vortex and a three-dimensional initialization disturbance. The mechanism behind of that is the resonance between the deformation field and the disturbance.
The occurrence of cooperative instabilities depend on the existance of initial perturbances. This means normally a sinusoidal amplitude which results from the superposition of two Kelvin waves A and B, if the Kelvin waves are reversed (m_A = -m_B), helix-shaped ($|m_A| = |m_B| = 1$), steady-state ($\omega_A - \omega_B = 0$) and if they have the same wave-number ($k_A - k_B = 0$).
If induced by atmospheric or boundary layer turbulence an amplitude of two parallel vortices occurs and if the decomposition of the perturbance into a finite number of Kelvin-waves includes two Kelvin-waves with the conditions denoted above a cooperative instability could be developed in the plane with maximum dilation. It was shown that this kind of parameter combinations for specified wave-numbers really exists. In the case of existance of other pairs of Kelvin-waves with wave-number different from k_A and the specific bounday conditions more cooperative instabilities may appear in parallel way. Water towing tank experiments have shown that long-wavelength and short-wavelength instabilities could exist in parallel.
In aircraft wakes mostly long-wavelength instabilities (Crow instabilitiy) could be observed by watching the condensation trail. The Crow instability exhibits only small growth rates and has in common wavelengths of about $5 < \lambda_{Crow}/b < 10$. It develops in planes with maximum deformation, i.e. the vortex amplitude grows in planes which are inclined by $\pm\pi/4$ against the horizontal plane. A projection of Crow instability into the xy-plane displays a symmetric and sinusoidal amplitude of the vortex axis, the projection into the xz-plane shows an in-phase amplitude.

5 Experimental studies

5.1 The F13 model

The DLR F13 model serve as a vortex generator which produces a specific two- or four-vortex system. In the current case the four-vortex-system is a counter-rotating four-vortex system.
The main wing of the F13 model has a span of b = 0,3 m and a chord length of c = 0,05 m.Thus the aspect ratio A_R

is 6 and the Angle of Attack α is 10°. The profile is a Wortmann FX63-137B-PT. This is a Low-Reynolds-Number-profile which was modified in Princeton-University. The horizontal tail wing (HTP) has the same profile parameters as the main wing but the chord length is c = 0,035 m and the span b = 0,09 m. To produce a counter-rotating 4-vortex system the Angle of Attack is -6°.
The Reynolds-number Re based on chord length of wing is 100000. The model is equiped with six rectangular flaps which can be moved independently. See FIG. 3 and FIG. 4 for detailed information.
The span- and circulation ratios are obtained from experimental PIV data taken in towing tank. In case of the calculations with HTP to produce a 4-vortex system the span ratio is b_1/b_2 = 0,3, the circulation ratio is Γ_1/Γ_2 = -0,4.
The periodical control of the flaps is done via a frequency generator which drives servo motors coming from aircraft modeling.

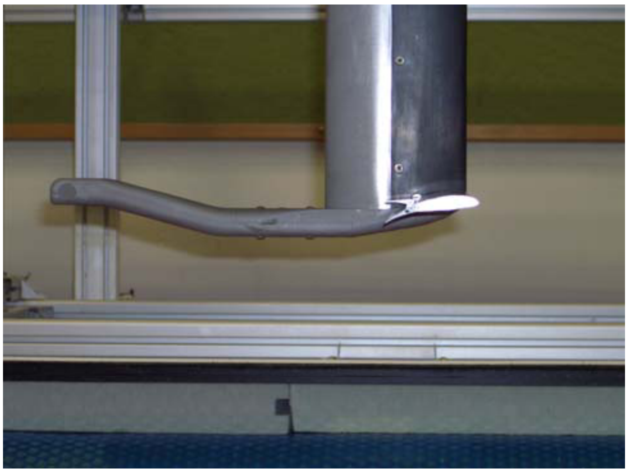

FIG. 3: F13 model with movable flaps in side view, flaps are deflected, no HTP mounted

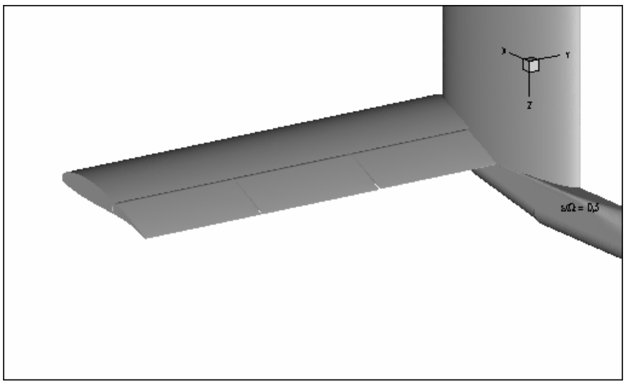

FIG. 4: Numerical F13 model, flaps in baseline configuration

5.2 The water towing tank

The water towing tank is a test facility which uses water as flow medium. This special experimental facility has the advantage of providing an incoming flow with very low disturbance levels due to the fact that the model is towed through still water.
The water towing tank consists of a water tank and a trolley supporting the model with its controlling instruments. The water tank has a total length of 18 m with a square cross section of 1,1 m x 1,1 m. It has ten pairs of glass windows allowing easy illumination for flow visualization and PIV measurements.
The measurement in the water towing tank were made in an Eulerian frame, i.e. the measurement plane remained fixed in the observation plane while the model is passing. Several magnetic switches are placed beside the rails for triggering instruments as well as for switching off and braking the trolley.
After settling down the water medium in the tank á free-stream turbulence close to zero can be assumed. The F13 model was towed through the quiet water just as an aeroplane wing moving through the still ambient atmosphere might do. The trolley was towed at a speed 2 m/s, for which the chord based Reynolds number is 100,000.

5.3 StereoPIV setup

A moving StereoPIV measurement system (Bao and Vollmers, 2005) was employed in order to obtain time-resolved cross-sectional flow fields of the descending wake vortex system. A laser light sheet, powered by a dual cavity Nd:YAG laser (max. pulse energy of 400mJ at 532nm with 5ns pulses), stretched over the full flow depth perpendicular to the tank axis. The water volume was seeded with hollow glass spheres with a mean diameter of 11microns and a density of 1.1 g/cm^3. Two high-resolution PIV cameras (ccd chip size of 1600px x 1200px, dynamic range 14bit gray-scale) acquired double-frame images of the illuminated seeding particles from both sides of the measurement plane (dual-side, forward-scattering, 45° off-axis arrangement). The cameras were attached to a carrier beam that was traversed downwards at a pre-set speed to follow the descending vortices in the developing wake. Large glass windows in the side walls and in the bottom of the tank allowed for convenient optical access. Using lenses of f = 35mm and f# 2.8, Scheimpflug adapters and air-glass-water transition prisms resulted in a field-of-view of 364,8 mm by 235,2 mm. A programmable sequencer synchronized the cameras with the pulsed laser light sheet and with the traversing system. Controlled by the sequencer, also the time delay between the laser double pulses was increased during a measurement run in order to account for the decreasing axial and azimuthal velocities in the evolving wake vortex system. The StereoPIV system was operated at a capturing frequency of 10Hz over a duration of up to 30s.

5.4 PIV evaluation of camera images

For calibration and stereo reconstruction, stereo images of a calibration grid in different positions were employed. In order to de-warp and map the stereo image recordings to reconstructed images onto a Cartesian grid, a ratio of first order polynomials was used as projection equation, and the necessary coefficients were evaluated. As to compensate for a possible slight misalignment between the plane of the calibration grid and the plane of the light sheet, a disparity correction has been performed on a set of particle images obtained from illumination with an especially thin light sheet.
The state-of-the-art PIV displacement algorithms employed a multi-pass multi-grid interrogation method with window deformation (e.g. Raffel et al., 1998), a multiple (Hart) correlation method, sub-pixel image shifting (image deformation) involving cubic B-splines, and peak detection based on Whittaker reconstruction. The multi-grid interrogation was performed by de-sampling of the images due to binning of neighboring pixels (Willert, 1997). The size of the final correlation window was 32px x 32px and 50% overlap, and resulted in time-resolved flow fields with more than 10,000 vectors. For outlier detection normalized median filtering (Westerweel and Scarano, 2005) and replacement by lower-order peaks was employed.

6 Numerical Studies

6.1 The TAU code

The numerical flow solver TAU is a finite volume method based on 3-dimensional Euler- and Navier-Stokes-equations. The calculation of a flow state in discrete points of an calculating domain asks for each point the definition of a capable control volume. Over the control volume the basical equations are integrated. Assuming constant flow values in each control volume the integration equation can be transferred into an easy sum equation.
Thus, the modification of the vector W of the dependent variable of a cell is equal to the flux Q through the cell side-faces reduced by a dissipation part to stabilize the method.

$$\frac{\Delta\vec{W}}{\Delta t} = -\frac{1}{V}\sum_{k=1}^{n}(\vec{Q}_k - \vec{D}_k) \tag{4}$$

V is the volume of the cell, n the number of the cell faces. The dissipation part is scaled with two constants $k^{(2)}$ and $k^{(4)}$. $k^{(2)}$ effects a stability in ... in which shocks occurs. The value $k^{(4)}$ makes sure that a global damping is available. Hence, in subsonic area this is the important parameter. Based on a arbitrary initial solution that discretized equations are integrated in discrete timesteps with an explicit multi-stage Runge-Kutta method over time until a steady flow field has set.
This ansatz goes back to the work of Jameson, Schmidt and Turkel. To initialize the calculation at all points of the grid pressure, density and velocity of free stream is set.

6.2 Validation of TAU Euler for nearfield calculation

The eligibility of TAU for wake vortex calculation with neglect of friction should be postulated and will be verified in the following part.
The methods for solution of the Euler equations doesn`t allow a realistic calculation of separation. For all considered geometries should be assumed that the surfaces don`t produce separation. In addition to that all geometries offer tips with sharp edges to avoid a strong Reynolds number dependency of vortex separation at wing and flap tips.
The work of Las and Longo has shown that in calculations based on Euler equations the contribution of vorticity on sharp edges is in order of realistic magnitude. Hence, a stable vortex with a realistic total pressure loss is formed. Similar to the work of Las et al. it can be found that the results of calculations with TAU solver with neglection if friction show a large dependency of local grid refinement. This determines the local active numerical dissipation. If the numerical dissipation is too strong the vortex will have a highly premature decay. Otherwise a too small numerical dissipation produces vortices with unrealisticly small vortex cores and too large circulation velocity. With decreasing numerical dissipation in calculations based on Euler equations the vortex approaches the structure of potential vortices and the simulated vortex tends to unrealistic vortex burst.

7 Configurations

Different configurations were used for numerical calculations and towing tank experiment.
Configuration 00 denotes the baseline configuration without flap moving, the other configurations are containing an outboard loading to trigger long wavelength instabilities like Crow. The configurations are listed in table 1 below.
In the towing tank a free stream velocity of 2 m/s were chosen in order to achieve a Reynolds-number of 100000 based on chord length of main wing. To ensure the comparability between TAU calculation and towing tank experiment the free stream velocity of calculations is set to 30 m/s (Ma 0,0874). This is nearly the minimum velocity which can be handled by TAU to give good results. In both cases incompressible boundary conditions

can be assumed. The change to comprssible flow conditions can be set to about Ma 0,2 which won`t be reached in these investigations. In contrast to the very small difference between Reynolds-numbers in water and air flow conditions is the large difference between Mach-numbers. The Mach-numer in air flow conditions is by factor 70 larger than the Mach-number in water flow environment. However, for comparability this will be negligible.
The frequencies which were chosen for flap motion are 0,8 and 1,0 Hz. Over the generalized reduced frequency

(5) $$f_{red} = \frac{2\pi f * l_{chord}}{v_\infty}$$

one can determine the frequency for air environment. Here 12 and 15 Hz respectively were calculated so the numerical unsteady calculations had to be done with these values.
TAB. 1 gives a list of chosen configurations, FIG. 5 and FIG. 6 show schematically the flap deflection of F13 model.

Config.	i/b flap (°)	m/b flap (°)	o/b flap (°)	freq. (Hz)	HTP ?
00n	0 / 0	0 / 0	0 / 0	--	no
01n	0 / -10	0 / -10	0 / 20	--	no
02n	0 / -10	0 / -10	0 / 20	12	no
03n	0 / 0	0 / 0	0 / 0	--	yes
04n	0 / -20	0 / 10	0 / 10	12	yes
05n	0 / -20	0 / 10	0 / 10	15	yes
00e	0 / 0	0 / 0	0 / 0	--	no
01e	0 / -10	0 / -10	0 / 20	--	no
02e	0 / -10	0 / -10	0 / 20	0,8	no

TAB. 1: Configurations of flap deflections and triggering frequencies

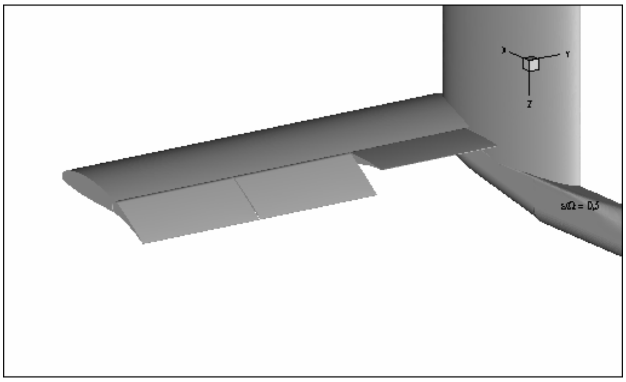

FIG. 5: Flap deflection for configuration 04n and 05n

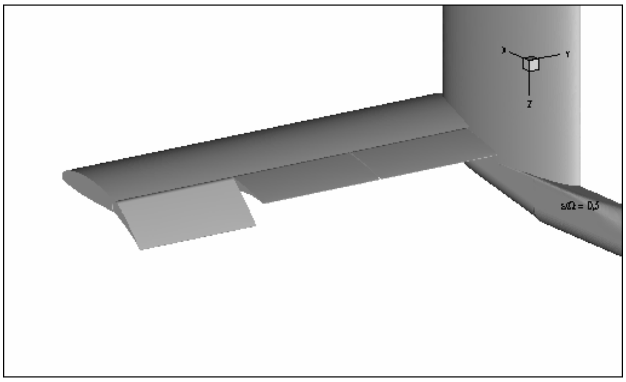

FIG. 6: Flap deflection for configuration 01n, 02n, 01e and 02e

8 Results

8.1 Numerical results

8.1.1 Baseline configuration

Two different configurations without flap deflection should be considered. FIG. 7 shows the iso-surfaces $s/\Omega = 0,5$. s/Ω is working as a filter for low-scaled vorticity parts and means the ratio of strain flow and vortex flow, see [16].
The smaller co-rotating vorticity tubes between main vortex and fuselage are shed from the flap gaps. Studies of calculations without flap gaps have shown that these vortices with small vorticity don`t have any influence on the development of main vortex and HTP vortex.

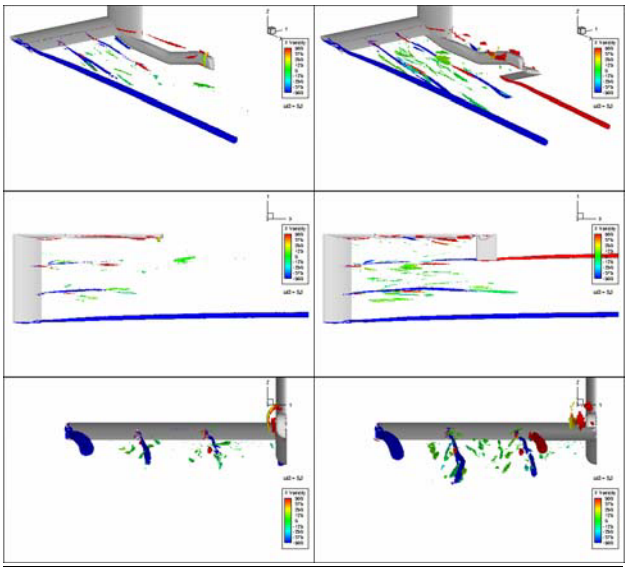

FIG. 7: Comparison Configuration 00n vs. 03n, colored by vorticity from -500 1/s to 500 1/s

8.1.2 Differential Flap Setting

Compared to the baseline case (conf. 00) the case with pre-selected deflected flaps yields results with more decay of the main vortex than in baseline case. The vortex pipe is considerably wider and within the boundary area the vortex is more frayed out (see FIG. 8).

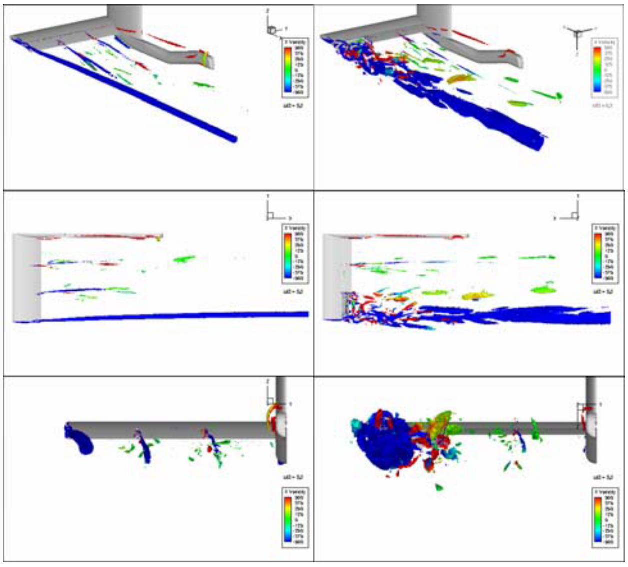

FIG 8: Comparison Configuration 00n vs. 01n, colored by vorticity from -500 1/s to 500 1/s

8.1.3 Oscillating Flap Setting

The results of calculations with HTP and periodically driven flaps have shown that there is an influence on vortex behaviour which depends obviously on triggering frequency. FIG. 9 indicates the difference of vortex development between frequency $f = 12$ Hz and $f = 15$ Hz. The frequencies can be found via generalized reduced frequeny as described in equation (5). This is a way to make numerical and experimental data comparible in this work.
Due to limited hardware resources for the unsteady calculations a compromise had to be found for choosing the best grid refinement. It would have been taken at least 25 to 30 Mill. grid points to come to a sufficient refinement with physical results. The effect which appears may come from something like end effects or side effects. That has its reason in a larger gradient in pressure and density with the consequence of more dissipation. Further studies with focal point on grid refine dependency have to be done to come to more exact results.

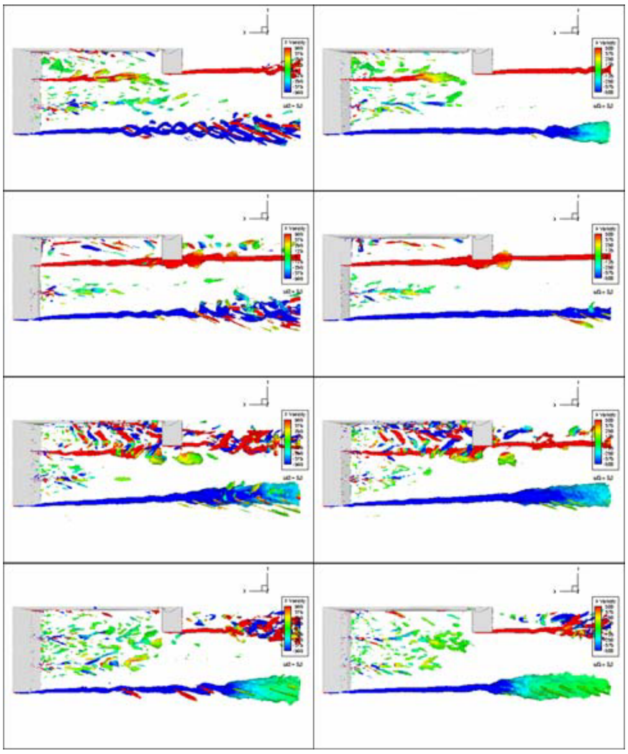

FIG 9: Comparison Configuration 04n vs. 05n, colored by vorticity from -500 1/s to 500 1/s

The direct comparison of undisturbed and oscillating disturbation as well as the comparison of steady deflected and oscillated moved flaps are shown in FIG. 10 and FIG. 11 respectively. Also here it is obvious that the decay of vortex tubes is accelerated when the configurative methods are applied to the model. This matter of fact was the base to chose the configuration for experimental studies.

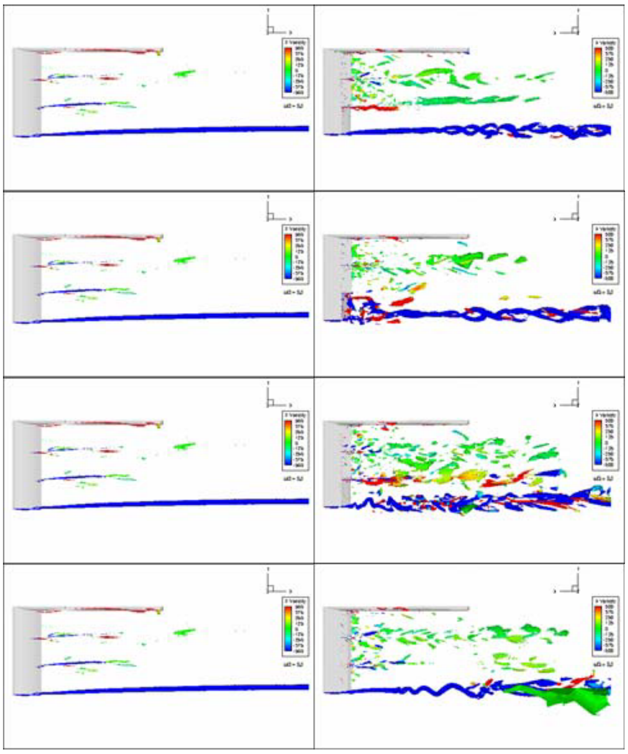

FIG 10: Comparison Configuration 00n vs. 02n, colored by vorticity from -500 1/s to 500 1/s

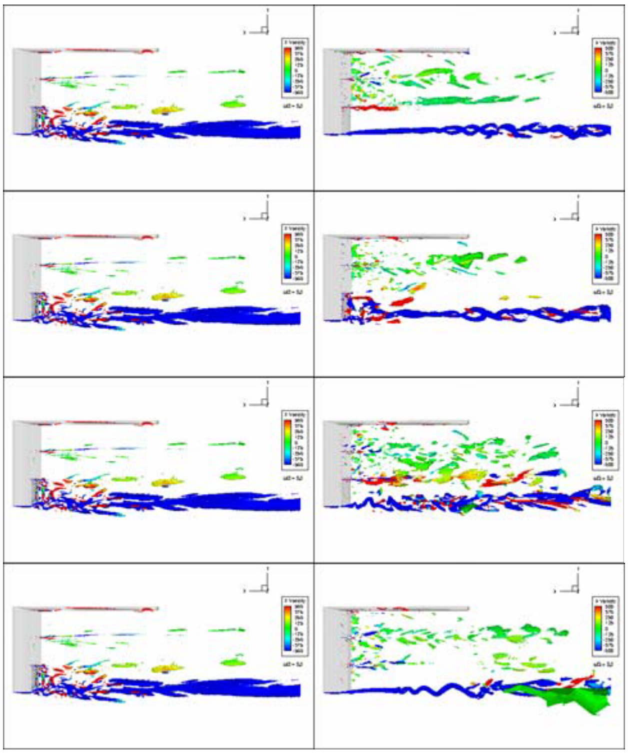

FIG 11: Comparison Configuration 01n vs. 02n, colored by vorticity from -500 1/s to 500 1/s

8.2 Experimental results

Three specific configurations will be discussed here. First the baseline configuration without HTP, the pre-selected flap deflection where the outboard flap is set to 20° and the other flaps are set to -10° to ensure lift neutrality.
Initially, in FIG. 12 the baseline case is compared with the pre-selected deflected flaps as denoted in configuration 01e. The analysis shows that there is an accelerated vortex mitigation as an effect of deflected flaps. The pictures are taken with a time interval of one second.
When the first picture was taken the counter-rotating flap vortex begins his rotation around the main vortex. That was expected according to the circulation ratio and the distance between the vortices. Three seconds after passing the measurement plane the smaller flap vortex has merged with the main vortex and there is only a small rest of vorticity with in the flow field.
FIG. 13 compares the baseline case (conf. 00e) with the oscillating flap setting case. The flap triggering frequency which was taken for this case is $f = 0{,}8$ Hz ([14,15]). To ensure that the flap deflection angle has always the same value while passing the measurement plane in every measurements the flap motion is started via triggering signal from the PIV measurement control. The results show that the influence of periodically oscillating flaps is also strong enough to bring the vortices to a premature decay. The direct comparison of pre-selected and oscillating moved flaps comes to the result that the vortex collapse is a little bit faster when the flaps are moved in a periodic way (see FIG. 14). All runs in water towing tank were very well reproducible

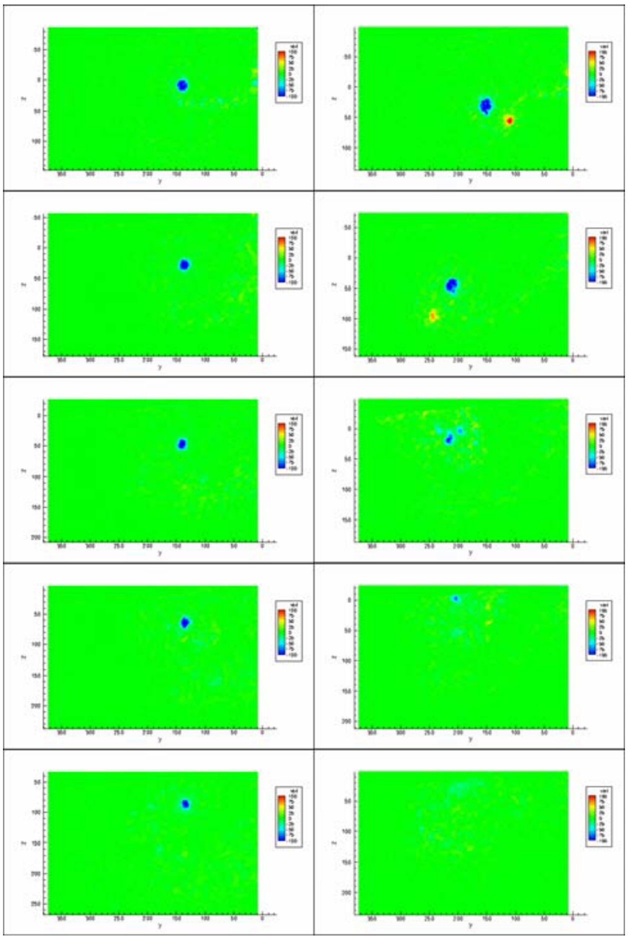

FIG 12: Comparison Configuration 00e vs. 01e, vorticity distribution from -100 1/s to 100 1/s is shown

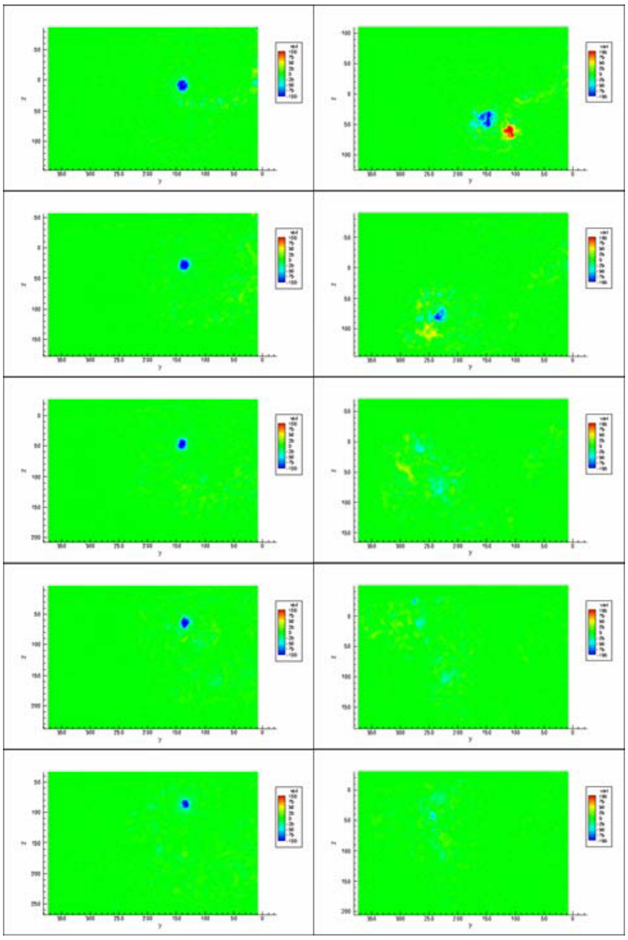

FIG 13: Comparison Configuration 00e vs. 02e, vorticity distribution from -100 1/s to 100 1/s is shown

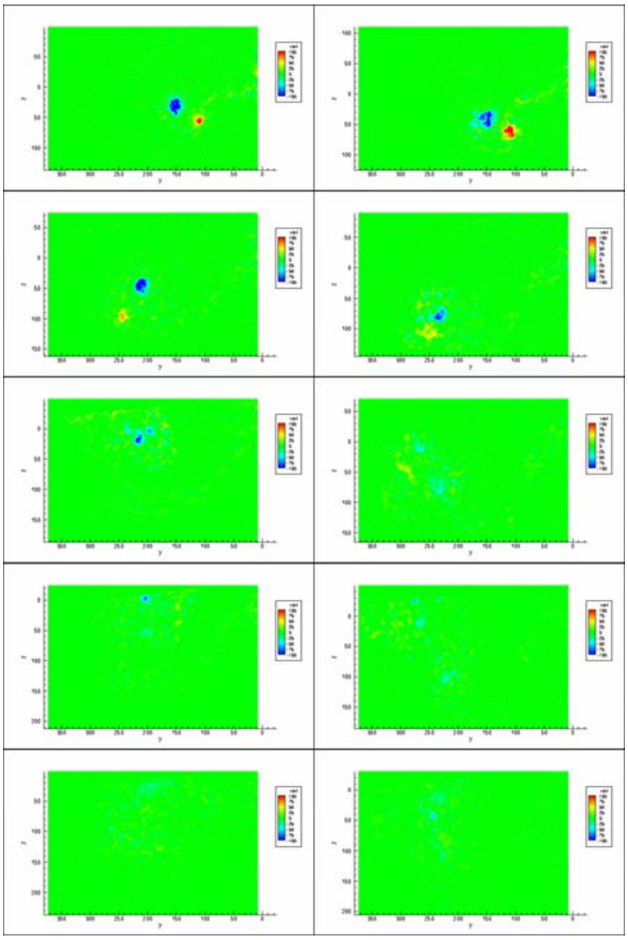

FIG 14: Comparison Configuration 02e vs. 01e, vorticity distribution from -100 1/s to 100 1/s is shown

9 Conclusions

The investigations have shown that it could be a promising way to achieve a premature vortex decay by using configurative methods on lift devices. Further grid studies have to be conducted to show if vortex bursting bases on some kind of end- or side-effects which is caused by too much dissipation in coarse grid regions.
Independent of that fact it is obvious that the magnitude of vortex bursting depends on triggering frequency. However, it is not yet clarified if this vortex behaviour shows the effect of long-wavelength instability triggering because this effect will be only observable in the far field. At that time there are not enough hardware resources available for such kind of unsteady calculations in the far field.
Experimental studies have shown that there is an effect when flaps are deflected or in motion with periodical shape. The effect seems to be somewhat stronger if flaps are in oscillating mode. Further studies have to be done to verify that.

10 References

[1] E. Stumpf, Investigations of 4-Vortex Systems for an Alleviation of Vortex Wakes and its Realization with Transport Aircraft, Doctoral Thesis RWTH Aachen, 2004
[2] M. Galle, Ein Verfahren zur numerischen Simulation kompressibler, reibungsbehafteter Strömungen auf hybriden Netzen, Doctoral Thesis, DLR-FB 99-04, 1999
[3] T. Gerhold, O.Friedrich, J. Evans, Calculations of Complex Three-dimensional Configurations Employing the DLR-τ-code, AIAA 97-0167, Reno, 1997
[4] A. Jameson, W. Schmidt, E. Turkel, Numerical Solutions of the Euler Equations by Finite Volume Methods Using Runge-Kutta Time Stepping Schemes, AIAA 81-1259, Palo Alto, 1981
[5] A. Jameson, Transonic Flow Calculations, MAE Report 1651, Princeton Unerversity, 1983
[6] T. Gerz, F. Holzäpfel, D. Darracq, Commercial aircraft wake vortices, Progress in Aerospace Science 38, 181-208, 2002
[7] L. Jacquin, D. Fabre, D. Sipp, V. Theofilis, H. Vollmers, Instability and unsteadiness of aircraft wake vortices, Aerospace Science and Technology 7, 577-593, 2003
[8] F. Bao, H. Vollmers, H. Mattner, Experimental Study on Controlling Wake Vortex in Water Towing Tank, ICIASF03, Göttingen, 2003
[9] E. Stumpf, Effect of Flap Strakes with regard to vortex wake alleviation, ECCOMAS2000, Barcelona, 2000
[10] E. Stumpf, R. Rudnik, A. Ronzheimer, Euler computations of the nearfield wake vortex of an aircraft in take-off configuration, Aerospace Science and Technology 4, 535-543, 2000
[11] E. Stumpf, J. Wild, A. A. Dafa´Alla, E. A. Meese, Numerical Simulations of the Wake Vortex Near Field of High Lift Configurations, ECCOMAS2004, Jyväskylä, 2004
[12] G. Voß, S. Melber-Wilkending, R. Rudnik, Premature Decay of Wake Vortices with Differential and Oscillating Flap Setting, ECCOMAS2006, Egmond aan Zee, 2006
[13] E. Stumpf, Numerical Study of Four-Vortex Aircraft Wakes
[14] S. Haverkamp, G.Neuwerth, D. Jacob, Active and Passive Vortex Wake Mitigation using Control Surfaces, Aerospace Science and Technology 9, 5-18, 2005
[15] S. Haverkamp, G.Neuwerth, D. Jacob, Studies on the Influence of Outboard Flaps on the Vortex Wake of a rectangular Wing, Aerospace Science and Technology 7, 331-339, 2003
[16] S. Melber, Wirbelkorrektur für Ein- und Zweigleichungs-Turbulenzmodelle und Implementation für das Spalart-Almaras Turbulenzmodell in den Strömungslöser DLR-TAU, IB 124 – 2002/17, 2002

[17] F. Bao, and H. Vollmers. Alleviation of end-effect in facilities for far wake investigations. 43rd AIAA Aerospace Sciences Meeting & Exhibit, Reno, NV, AIAA 2005-0907, 2005
[18] M. Raffel, C. E. Willert, and J. Kompenhans. Particle image velocimetry. A practical guide. Springer, Berlin Heidelberg New York, 1998
[19] J. Westerweel and F. Scarano. Universal outlier detection for PIV data. Exp Fluids, V39(6):1096-1100, Dec. 2005
[20] C. Willert. Stereoscopic digital particle image velocimetry for application in wind tunnel flows. Meas Sci Technol, 8:1465-1479, 1997